

A massive quiescent galaxy at redshift 4.658

Adam C. Carnall^{1*}, Ross J. McLure¹, James S. Dunlop¹, Derek J. McLeod¹, Vivienne Wild², Fergus Cullen¹, Dan Magee³, Ryan Begley¹, Andrea Cimatti^{4,5}, Callum T. Donnan¹, Massissilia L. Hamadouche¹, Sophie M. Jewell¹ and Sam Walker¹

¹Institute for Astronomy, School of Physics & Astronomy, University of Edinburgh, Royal Observatory, Edinburgh, EH9 3HJ, UK.

²School of Physics & Astronomy, University of St Andrews, North Haugh, St Andrews, KY16 9SS, UK.

³Department of Astronomy and Astrophysics, UCO/Lick Observatory, University of California, Santa Cruz, CA 95064, USA.

⁴Department of Physics and Astronomy (DIFA), University of Bologna, Via Gobetti 93/2, I-40129, Bologna, Italy.

⁵INAF, Osservatorio di Astrofisica e Scienza dello Spazio, Via Piero Gobetti 93/3, I-40129, Bologna, Italy.

*Corresponding author email: adam.carnall@ed.ac.uk

Abstract

We report the spectroscopic confirmation of a massive quiescent galaxy, GS-9209 at a new redshift record of $z = 4.658$, just **1.25** Gyr after the Big Bang, using new deep continuum observations from JWST NIR-Spec. From our full-spectral-fitting analysis, we find that this galaxy formed its stellar population over a $\simeq 200$ Myr period, approximately **600 – 800** Myr after the Big Bang ($z_{\text{form}} = 7.3 \pm 0.2$), before quenching at $z_{\text{quench}} = 6.7 \pm 0.3$. GS-9209 demonstrates unambiguously that massive galaxy formation was already well underway within the first billion years of cosmic history, with this object having reached a stellar mass of $\log_{10}(M_*/M_\odot) > 10.3$ by $z = 7$. This galaxy also clearly demonstrates that the earliest onset of galaxy quenching was no later than $\simeq 800$ Myr after the Big Bang. We estimate the iron abundance and α -enhancement of GS-9209, finding $[\text{Fe}/\text{H}] = -0.97^{+0.06}_{-0.07}$ and $[\alpha/\text{Fe}] = 0.67^{+0.25}_{-0.15}$, suggesting the stellar mass vs iron abundance relation at $z \simeq 7$, when this object formed most of its stars, was $\simeq 0.4$ dex lower than at $z \simeq 3.5$. Whilst its spectrum is dominated by stellar emission, GS-9209 also exhibits broad $\text{H}\alpha$ emission, indicating that it hosts an active galactic nucleus (AGN), for which we measure a black-hole

2 *A massive quiescent galaxy at redshift 4.658*

mass of $\log_{10}(M_{\bullet}/M_{\odot}) = 8.7 \pm 0.1$. Although large-scale star formation in GS-9209 has been quenched for almost half a billion years, the significant integrated quantity of accretion implied by this large black-hole mass suggests AGN feedback plausibly played a significant role in quenching star formation in this galaxy. GS-9209 is also extremely compact, with an effective radius of just 215 ± 20 parsecs. This intriguing object offers perhaps our deepest insight yet into massive galaxy formation and quenching during the first billion years of cosmic history.

1 Summary

The discovery of massive galaxies with old stellar populations at early cosmic epochs has historically acted as a key constraint on models for both galaxy formation physics and cosmology [1–4]. Today, the extremely rapid assembly of the earliest galaxies during the first billion years of cosmic history continues to challenge our understanding of galaxy formation physics [5, 6]. The advent of the James Webb Space Telescope (JWST) has exacerbated this issue by confirming the existence of galaxies in significant numbers as early as the first few hundred million years [7–9]. Perhaps even more surprisingly, in some galaxies, this initial highly efficient star formation rapidly shuts down, or quenches, giving rise to massive quiescent galaxies as little as ~ 1.5 billion years after the Big Bang, at redshifts up to $z \simeq 4$ [4, 10]. Due to their faintness and red colour, it has proven extremely challenging to learn about these extreme quiescent galaxies, or to confirm whether any exist at earlier times. Here, we report the spectroscopic confirmation of a quiescent galaxy, GS-9209, at a new redshift record of 4.658, just 1.25 billion years after the Big Bang, using the NIRSpec instrument on JWST. The transformative power of JWST allows us to characterise the physical properties of this early massive galaxy in unprecedented detail. GS-9209 has a stellar mass of $M_* = 4.1 \pm 0.2 \times 10^{10} M_{\odot}$, and quenched star formation at $z = 6.7 \pm 0.3$, when the Universe was $\simeq 800$ million years old. This intriguing object offers perhaps our deepest insight yet into massive galaxy formation and quenching during the first billion years of cosmic history.

2 Results

GS-9209 was first highlighted in the early 2000s as an object with red optical to near-infrared colours and a photometric redshift of $z \simeq 4.5$ [11]. An optical spectrum was taken in the mid-2010s as part of the VIMOS Ultra Deep Survey (VUDS) [12], showing tentative evidence for a Lyman break at $\lambda \simeq 7000\text{\AA}$, but no Lyman α emission. During the past 5 years, several studies have identified GS-9209 as a candidate high-redshift massive quiescent galaxy [13, 14], based on its blue colours at wavelengths, $\lambda = 2 - 8\mu\text{m}$ and non-detection at millimetre wavelengths [15]. GS-9209 is also not detected in X-rays [16], at radio wavelengths [17], or at $\lambda = 24\mu\text{m}$ [18]. The faint, red nature of the source (with magnitudes $H_{\text{AB}} = 24.7$ and $K_{\text{AB}} = 23.6$) means that near-infrared spectroscopy with ground-based instrumentation is prohibitively expensive.

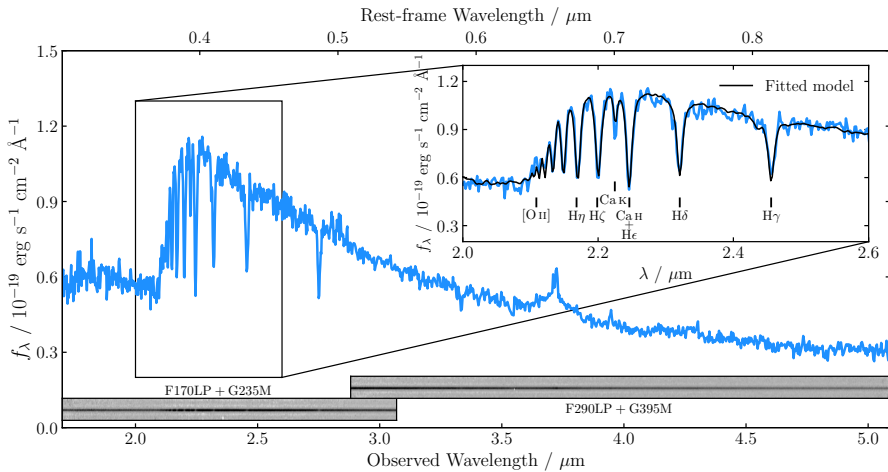


Fig. 1 JWST NIRSpec observations of GS-9209. Data were taken using the G235M and G395M gratings ($R = 1000$), providing wavelength coverage from $\lambda = 1.7 - 5.1\mu\text{m}$. The galaxy is at $z = 4.658$, and exhibits extremely deep Balmer absorption lines, similar to lower redshift post-starburst galaxies, clearly indicating this galaxy experienced a significant, rapid drop in star-formation rate (SFR) within the past few hundred million years. The spectral region from $\lambda = 2.6 - 4.0\mu\text{m}$, containing $H\beta$ and $H\alpha$, is shown at a larger scale in Fig. 2.

2.1 Spectroscopic data

On 16th November 2022, we obtained medium-resolution spectroscopy ($R = \lambda/\Delta\lambda = 1000$) through the JWST NIRSpec fixed slit, integrating for 3 hours with the G235M grism and 2 hours with the G395M grism, providing continuous wavelength coverage from $\lambda = 1.7 - 5.1\mu\text{m}$. These data, shown in Fig. 1, reveal a full suite of extremely deep Balmer absorption features, from which we measure a spectroscopic redshift of 4.6582 ± 0.0002 , consistent with previous photometric data and the VUDS spectrum. The spectrum strongly resembles that of an A-type star, and is reminiscent of lower-redshift post-starburst galaxies [19–21], with a $H\delta_A$ equivalent width (EW), as measured by the $H\delta_A$ Lick index, of $7.9 \pm 0.3\text{\AA}$, comparable to the most extreme values observed in the local Universe [22]. These spectral features strongly indicate this galaxy has undergone a sharp decline in star-formation rate (SFR) during the preceding few hundred Myr.

The observed continuum is relatively smooth, as is the case for A-type stars, with only two clearly detected metal absorption features: the Ca K line at 3934\AA and the Na D feature at 5895\AA . The Ca H line at 3969\AA is blended with the much stronger He ϵ Balmer line. The spectrum exhibits only the merest suspicion of [O II] 3727\AA and [O III] 4959\AA , 5007\AA emission, and no apparent infilling of $H\beta$ or any of the higher-order Balmer absorption lines. However, as can be seen in Fig. 2, both $H\alpha$ and [N II] 6584\AA are clearly albeit weakly detected in emission, with $H\alpha$ also exhibiting an obvious broad component. This broad component, along with the relative strength of [N II] compared with the narrow $H\alpha$ line indicate the presence of an accreting supermassive

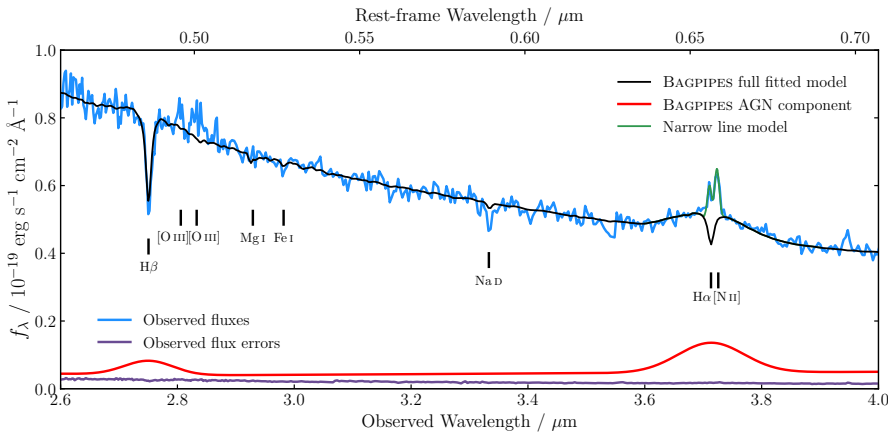


Fig. 2 JWST NIRSpec observations of GS-9209: zoom in on $\text{H}\beta$ and $\text{H}\alpha$. Data are shown in blue, with their associated uncertainties visible at the bottom in purple. The full Bagpipes fitted model is shown in black, with the AGN component shown in red. The narrow $\text{H}\alpha$ and $[\text{N II}]$ lines were masked during the Bagpipes fitting process, and subsequently fitted with Gaussian functions, shown in green. Key emission and absorption features are also marked.

black hole: an active galactic nucleus (AGN). However, the extreme EWs of the observed Balmer absorption features indicate that the continuum emission must be strongly dominated by the stellar component. Nevertheless, the AGN contribution to GS-9209 must be carefully modelled when fitting the spectrum of this source to extract reliable stellar population properties (see Section 4.3).

2.2 Full spectral fitting

To measure the stellar population properties of GS-9209, we perform full spectrophotometric fitting using the Bagpipes code. Full details of the methodology we employ are given in Section 4.3. Briefly, we combine our spectroscopic data with previously available CANDELS photometry, as well as new JWST NIRCam medium-band imaging in 5 filters from the Ultra Deep Field Medium-Band Survey (Programme ID: 1963; PI: Williams). We first mask the wavelengths corresponding to $[\text{O II}]$, $[\text{O III}]$, narrow $\text{H}\alpha$ and $[\text{N II}]$, due to likely AGN contributions. We discuss the properties of these lines and their likely origin in Section 2.5. We then fit a 22-parameter model for the stellar, dust, nebular and AGN components, as well as spectrophotometric calibration.

The resulting posterior median model is shown in black in Figs 1 and 2. We obtain a stellar mass of $\log_{10}(M_*/\text{M}_\odot) = 10.61 \pm 0.02$, under the assumption of a Kroupa initial mass function (IMF) [23]. We additionally recover a very low level of dust attenuation, with $A_V = 0.04^{+0.05}_{-0.03}$. The SFR we measure averaged over the past 100 Myr is consistent with zero, with a very stringent upper bound, though this is largely a result of our chosen star-formation history (SFH) parameterisation [24]. We report a more-realistic upper bound on the SFR in Section 2.5 based on the narrow $\text{H}\alpha$ line.

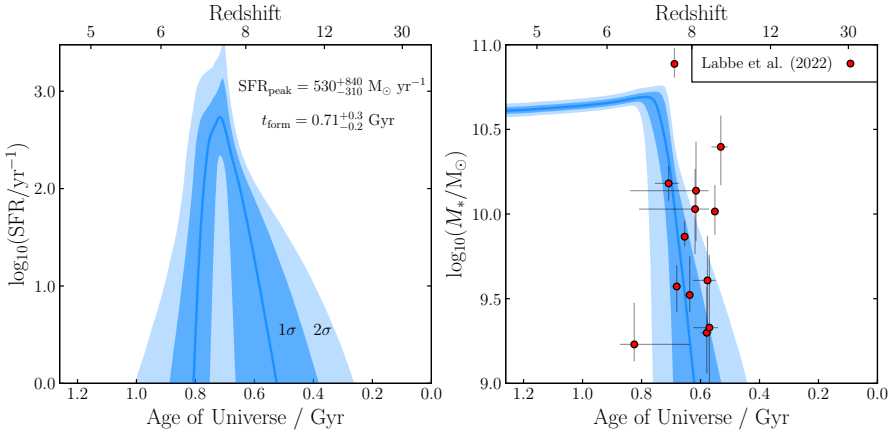


Fig. 3 The star-formation history of GS-9209. The SFR as a function of time is shown in the left panel, with the stellar mass as a function of time shown in the right panel. The blue lines show the posterior medians, with the darker and lighter shaded regions showing the 1σ and 2σ confidence intervals respectively. We find a formation redshift, $z_{\text{form}} = 7.3 \pm 0.2$ and a quenching redshift, $z_{\text{quench}} = 6.7 \pm 0.3$. The sample of massive $z \simeq 8$ galaxy candidates from JWST CEERS reported by [7] is also shown in the right panel, demonstrating that these candidates are plausible progenitors for GS-9209.

2.3 Star-formation history

The star-formation history (SFH) we recover is shown in Fig. 3. We find that GS-9209 formed its stellar population largely during a $\simeq 200$ Myr period, from around 600 – 800 Myr after the Big Bang ($z \simeq 7 - 8$). We recover a mass-weighted mean formation time, $t_{\text{form}} = 0.71^{+0.03}_{-0.02}$ Gyr after the Big Bang, corresponding to a formation redshift, $z_{\text{form}} = 7.3 \pm 0.2$. This is the redshift at which GS-9209 would have had half its current stellar mass, approximately $\log_{10}(M_*/M_\odot) = 10.3$. We find that GS-9209 quenched (which we define as the time at which its sSFR fell below 0.2 divided by the Hubble time, e.g., [25]) at time $t_{\text{quench}} = 0.79^{+0.06}_{-0.04}$ Gyr after the Big Bang, corresponding to a quenching redshift, $z_{\text{quench}} = 6.7 \pm 0.3$.

Our model predicts that the peak historical SFR for GS-9209 (at approximately z_{form}) was within the range $\text{SFR}_{\text{peak}} = 530^{+840}_{-310} \text{ M}_\odot \text{ yr}^{-1}$. This is similar to the SFRs of bright submillimetre galaxies (SMGs). The number density of SMGs with $\text{SFR} > 300 \text{ M}_\odot \text{ yr}^{-1}$ at $5 < z < 6$ has been estimated to be $\simeq 3 \times 10^{-6} \text{ Mpc}^{-3}$ [26]. Extrapolation then suggests that the SMG number density at $z \simeq 7$ is $\simeq 1 \times 10^{-6} \text{ Mpc}^{-3}$, which equates to $\simeq 1$ SMG at $z \simeq 7$ over the $\simeq 400$ square arcmin area from which GS-9209 and one other $z > 4$ quiescent galaxy were selected [14]. This broadly consistent number density suggests it is entirely plausible that GS-9209 went through a SMG phase at $z \simeq 7$, shortly before quenching.

In the right panel of Fig. 3, we show the positions of the massive, high-redshift galaxies recently reported by [7] in the first imaging release from the JWST CEERS survey. It can be seen that the positions of these galaxies are

6 *A massive quiescent galaxy at redshift 4.658*

broadly consistent with the SFH of GS-9209 at $z \simeq 8$. It should however be noted that, as previously discussed, GS-9209 was selected as one of only two robustly identified $z > 4$ massive quiescent galaxies in an area roughly 10 times the size of the initial CEERS imaging area [14]. It therefore seems unlikely that a large fraction of the objects reported by [7] will evolve in a similar way to GS-9209 over the redshift interval from $z \simeq 5 - 8$.

2.4 Stellar metallicity

We obtain a relatively low stellar metallicity for GS-9209 of $\log_{10}(Z_*/Z_\odot) = -0.97^{+0.06}_{-0.07}$ (where we adopt a value of $Z_\odot = 0.0142$ [27]). By re-running our fitting procedure at a range of fixed metallicity values, we find that metallicity is constrained mainly by the shape of the stellar continuum emission above the Balmer break (the $\lambda = 2.0 - 2.6\mu\text{m}$ region shown in the inset panel of Fig. 1), which is strongly incompatible with models at higher metallicities. This UV continuum shape is mostly sensitive to the Fe abundance [28, 29], and we therefore associate our measured Z_* value with the Fe abundance, $[\text{Fe}/\text{H}] = -0.97^{+0.06}_{-0.07}$. This is $\simeq 0.4$ dex below the mean $z \simeq 3.5$ stellar mass vs iron abundance relationship for star-forming galaxies [30]. Given that GS-9209 formed its stellar population at $z \simeq 7$, our result suggests that the stellar mass vs iron abundance relation continues to trend downwards over the redshift interval from $z \simeq 3.5 - 7$, as is observed between the local Universe and $z \simeq 3.5$.

As can be seen from Figs 1 and 2, we do not obtain a good fit to either the Ca K or Na D absorption features, with our model significantly under-predicting the depths of both. Stellar populations that form and quench rapidly are known to be α -enhanced [31], whereas the stellar population models we fit assume a fixed scaled-Solar abundance pattern (see Section 4.3). We therefore provisionally attribute the failure of our model to reproduce these α -element absorption features to significant α -enhancement in GS-9209. It should be noted however that both of these features (in particular Na D) can also arise from interstellar medium (ISM) absorption, though the low dust attenuation we infer from our spectral fit might be taken to suggest this effect should be small.

Unfortunately, reliable empirical α -enhanced models are not currently available for stellar populations with ages less than 1 Gyr. Therefore, to test this α -enhancement hypothesis, we first measure the EWs of these two features from our data (see Section 4), obtaining a Ca K EW of $2.15 \pm 0.25\text{\AA}$, and a Na D EW of $2.09 \pm 0.46\text{\AA}$. For comparison, our posterior median model predicts values of 1.12\AA and 0.41\AA respectively. We then scale up the metallicity of our model, keeping all other parameters fixed, until the predicted EWs match our data. By this process, we obtain $[\text{Ca}/\text{Fe}] = 0.67^{+0.25}_{-0.15}$. We are however unable to reproduce the observed depth of Na D via this process, which we attribute to the known strong ISM component of this absorption feature [29, 32]. The Ca abundance we calculate is however fully consistent with both theoretical predictions [33] and observational evidence [34] for α -enhancement in extreme stellar populations. In particular, [3] report a consistent value of $[\text{Ca}/\text{Fe}] = 0.59 \pm 0.07$ for an extreme massive quiescent galaxy at $z = 2.1$.

We therefore adopt our measured Ca abundance as our best estimate of the α -enhancement of GS-9209, $[\alpha/\text{Fe}] = 0.67^{+0.25}_{-0.15}$. This extreme α -enhancement supports our finding of an extremely short, $\lesssim 200$ Myr formation timescale [31], as shown in Fig. 3. We caution however that this value could be artificially boosted by an ISM contribution to the Ca K absorption line.

2.5 Evidence for AGN activity

From our Bagpipes full spectral fit, we measure an observed broad H α flux of $f_{\text{H}\alpha, \text{broad}} = 1.26 \pm 0.08 \times 10^{-17} = \text{erg s}^{-1} \text{cm}^{-2}$ and full width at half maximum (FWHM) of $10800 \pm 600 \text{ km s}^{-1}$ in the rest frame. This line width, whilst very broad, is consistent with rest-frame UV broad line widths measured for some $z = 6$ quasars (e.g., [35, 36]).

We also recover an observed AGN continuum flux at rest-frame wavelength, $\lambda_{\text{rest}} = 5100\text{\AA}$ of $f_{5100} = 0.040 \pm 0.004 \times 10^{-19} \text{ erg s}^{-1} \text{cm}^{-2} \text{\AA}^{-1}$. This is approximately 5 per cent of the total observed flux from GS-9209 at $\lambda = 2.9\mu\text{m}$. We measure a power-law index for the AGN continuum emission of $\alpha_\lambda = -1.36 \pm 0.08$ at $\lambda_{\text{rest}} < 5000\text{\AA}$, and $\alpha_\lambda = 0.69 \pm 0.14$ at $\lambda_{\text{rest}} > 5000\text{\AA}$. These indices are broadly consistent with the average values observed for local quasars [37]. In combination with the non-detection of GS-9209 at longer wavelengths (see Section 2), this suggests the AGN component in GS-9209 is not significantly reddened. The AGN contribution to the continuum flux from GS-9209 rises to $\simeq 15$ per cent at the blue end of our spectrum ($\lambda = 1.7\mu\text{m}$), and $\simeq 20$ per cent at the red end ($\lambda = 5\mu\text{m}$). Just above the Lyman break at $\lambda \simeq 7000\text{\AA}$, the AGN contribution is $\simeq 35$ per cent of the observed flux.

Given our measured $f_{\text{H}\alpha, \text{broad}}$, which is more direct than our AGN continuum measurement, the average relation for local AGN presented by [38] predicts f_{5100} to be $\simeq 0.4$ dex brighter than we measure. However, given the intrinsic scatter of 0.2 dex they report, our measured f_{5100} is only 2σ below the mean relation. The extreme equivalent widths of the observed Balmer absorption features firmly disfavour stronger AGN continuum emission.

We fit the narrow H α and [N II] lines in our spectrum as follows. We first subtract from our observed spectrum the posterior median Bagpipes model from our full spectral fitting, described in Section 2.2. We then simultaneously fit Gaussian components to both lines, assuming the same velocity width for both, which is allowed to vary. This process is visualised in Fig. 2. We also show the broad H β line in our AGN model, for which we assume the same width as broad H α , as well as Case B recombination. It can be seen that the broad H β line peaks at around the noise level in our spectrum, and is hence too weak to be clearly observed in our data.

We obtain a H α narrow-line flux of $1.58 \pm 0.10 \times 10^{-18} \text{ erg s}^{-1} \text{cm}^{-2}$ and a [N II] flux of $1.56 \pm 0.10 \times 10^{-18} \text{ erg s}^{-1} \text{cm}^{-2}$, giving a line ratio of $\log_{10}([\text{N II}]/\text{H}\alpha) = -0.01 \pm 0.04$. This line ratio is significantly higher than would be expected as a result of ongoing star formation, and is consistent with excitation due to an AGN or shocks resulting from galactic outflows [39]. Such outflows are commonly observed in post-starburst galaxies at $z \gtrsim 1$ [40].

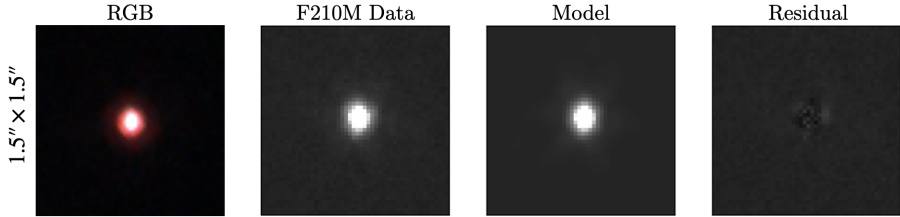


Fig. 4 JWST NIRCam imaging of GS-9209. Each cutout image shows an area of $1.5'' \times 1.5''$. The RGB image in the first (leftmost) panel is constructed with F430M as red, F210M as green and F182M as blue. The second panel shows the F210M image, with our posterior median PetroFit model shown in the third panel. The residuals between model and data are shown in the right panel, on the same colour scale as the middle two panels.

without corresponding AGN signatures, suggesting either that these outflows are driven by stellar feedback, or that the AGN activity responsible for the outflow has since shut down.

Even if we assume all the narrow H α emission is driven by ongoing star formation, we obtain $\text{SFR} = 1.9 \pm 0.1 \text{ M}_\odot \text{ yr}^{-1}$ [41], corresponding to $\log_{10}(\text{sSFR/yr}^{-1}) = -10.3 \pm 0.1$. This is under the assumption that dust attenuation is negligible, based on our finding of a very low A_V from full spectral fitting in Section 2.2. This is well below the commonly applied sSFR threshold for defining quiescent galaxies at this redshift [25], $\log_{10}(\text{sSFR}_{\text{threshold}}/\text{yr}^{-1}) = 0.2/t_{\text{H}} = -9.8$, where t_{H} is the age of the Universe. Given the multiple lines of evidence we uncover for a significant non-stellar component to this line, it is likely that the SFR of GS-9209 is considerably lower than this estimate.

We estimate the black-hole mass for GS-9209, M_\bullet , from our combined H α flux and broad-line width, using the relation presented in Equation 6 of [38], obtaining $\log_{10}(M_\bullet/\text{M}_\odot) = 8.7 \pm 0.1$. From our Bagpipes full spectral fit, we infer a stellar velocity dispersion, $\sigma = 247 \pm 16 \text{ km s}^{-1}$ for GS-9209, after correcting for the intrinsic dispersion of our template set, as well as instrumental dispersion. Given this measurement, the relationship between velocity dispersion and black-hole mass presented by [42] predicts $\log_{10}(M_\bullet/\text{M}_\odot) = 8.9 \pm 0.1$.

Given the broad agreement between these estimators, it seems reasonable to conclude that GS-9209 contains a supermassive black hole with a mass of approximately half a billion to a billion Solar masses. It is interesting to note that this is $\simeq 4 - 5$ times the black-hole mass that would be expected given the stellar mass of the galaxy, assuming this is equivalent to the bulge mass. This is consistent with the observed increase in the average black-hole to bulge mass ratio for massive galaxies from $0 < z < 2$ [43]. This large amount of historical AGN accretion relative to star formation strongly implies that AGN feedback may be responsible for quenching this galaxy.

2.6 Size measurement and dynamical mass

GS-9209 is an extremely compact source, which is only marginally resolved in the highest-resolution available imaging data. The CANDELS/3DHST team

[44] measured an effective radius, $r_e = 0.029 \pm 0.002''$ for GS-9209 in the HST F125W filter via Sérsic fitting, along with a Sérsic index, $n = 6.0 \pm 0.8$. At $z = 4.658$, this corresponds to $r_e = 189 \pm 13$ parsecs.

We update this size measurement using the newly available JWST NIRCam F210M-band imaging, which has a FWHM of $\simeq 0.07''$ (see Section 4.4). Accounting for the AGN point-source contribution, we measure an effective radius, $r_e = 0.033 \pm 0.003''$ for the stellar component of GS-9209, along with a Sérsic index, $n = 2.3 \pm 0.3$. At $z = 4.658$, this corresponds to $r_e = 215 \pm 20$ parsecs. This is consistent with the CANDELS/3DHST measurement, and is $\simeq 0.7$ dex below the mean relationship between r_e and stellar mass for quiescent galaxies at $z \simeq 1$ [44, 45]. This is interesting given that post-starburst galaxies $z \simeq 1$ are known to be more compact than is typical for the wider quiescent population [46]. We calculate a stellar-mass surface density within r_e of $\log_{10}(\Sigma_{\text{eff}}/\text{M}_\odot \text{ kpc}^{-2}) = 11.15 \pm 0.08$, consistent with the densest stellar systems in the Universe [47]. We show the F210M data for GS-9209, along with our posterior-median model in Fig. 4.

We estimate the dynamical mass using our size and velocity dispersion measurements (e.g., [40]), obtaining a value of $\log_{10}(M_{\text{dyn}}/\text{M}_\odot) = 10.3 \pm 0.1$. This is $\simeq 0.3$ dex lower than the stellar mass we measure. As GS-9209 is only marginally resolved, even in JWST imaging data, and due to the presence of the AGN component, it is plausible that our measured r_e may be subject to systematic uncertainties. Deeper imaging data in the F200W or F277W bands (e.g., from the JWST Advanced Deep Extragalactic Survey; JADES) will provide a useful check on this, particularly given the lower AGN fraction in the F277W band. Furthermore, since the pixel scale of NIRSpec is $0.1''$, our velocity dispersion measurement may not accurately represent the central velocity dispersion of GS-9209, leading to an underestimated dynamical mass. It should also be noted that the stellar mass we measure is strongly dependent on our assumed IMF.

A final, intriguing possibility would be a high level of rotational support in GS-9209, as has been observed for quiescent galaxies at $2 < z < 3$ [48]. Unfortunately, the extremely compact nature of the source makes any attempt at resolved studies extremely challenging, even with the JWST NIRSpec integral field unit. Resolved kinematics for this galaxy would be a clear use case for the High Angular Resolution Monolithic Optical and Near-infrared Integral field spectrograph (HARMONI) planned for the Extremely Large Telescope (ELT).

3 Conclusion

We report the spectroscopic confirmation of a massive quiescent galaxy, GS-9209 at a new redshift record of $z = 4.6582 \pm 0.002$, with a stellar mass of $\log_{10}(M_*/\text{M}_\odot) = 10.61 \pm 0.02$. This galaxy formed its stellar population over a $\simeq 200$ Myr period, approximately 600 – 800 Myr after the Big Bang ($z_{\text{form}} = 7.3 \pm 0.2$), before quenching at $z_{\text{quench}} = 6.7 \pm 0.3$. GS-9209 demonstrates unambiguously that massive galaxy formation was already well

underway within the first billion years of cosmic history, with this object having reached $\log_{10}(M_*/M_\odot) > 10.3$ by $z = 7$. This galaxy also clearly demonstrates that the earliest onset of galaxy quenching was no later than $\simeq 800$ Myr after the Big Bang.

We estimate the iron abundance and α -enhancement of GS-9209, finding $[\text{Fe}/\text{H}] = -0.97^{+0.06}_{-0.07}$ and $[\alpha/\text{Fe}] = 0.67^{+0.25}_{-0.15}$, suggesting the stellar mass vs iron abundance relation at $z \simeq 7$, when this object formed most of its stars, was $\simeq 0.4$ dex lower than at $z \simeq 3.5$ [30]. Whilst its spectrum is dominated by stellar emission, GS-9209 also hosts an AGN, for which we measure a black-hole mass of $\log_{10}(M_\bullet/M_\odot) = 8.7 \pm 0.1$ from the observed broad and narrow H α emission [38]. We also predict a consistent value of $\log_{10}(M_\bullet/M_\odot) = 8.9 \pm 0.1$ based on the stellar velocity dispersion of GS-9209 [42]. Whilst large-scale star formation in GS-9209 has been quenched for almost half a billion years, the significant integrated quantity of AGN accretion implied by this large black-hole mass ($\simeq 4 - 5$ times what would be expected given the stellar mass of this galaxy) suggests that AGN activity plausibly played a significant role in quenching star formation in this galaxy.

Based on the properties we measure, GS-9209 seems likely to be associated with the most extreme galaxy populations currently known at $z > 5$, such as the highest-redshift submillimetre galaxies and quasars (e.g., [36, 49, 50]). GS-9209 is also plausibly descended from an object similar to the $z \simeq 8$ massive galaxy candidates recently reported in the first data from the JWST CEERS programme [7], though the number density of these candidates is significantly higher than that of $z > 4$ quiescent galaxies. GS-9209 and similar objects (e.g., [9]) are also likely progenitors for the dense, ancient cores of the most massive galaxies in the local Universe.

This study, which makes use of just 5 hours of on-source integration time, demonstrates the huge potential of JWST for revolutionising our understanding of the high-redshift Universe. It seems clear that this work will be followed rapidly by the confirmation and detailed spectroscopic exploration of large samples of $z > 4$ quiescent galaxies, to build up a detailed understanding of massive galaxy formation and quenching during the first billion years.

4 Methods

4.1 Spectroscopic data reduction

We reduce our NIRSpec data using the JWST Science Calibration Pipeline v1.8.4, using version 1017 of the JWST calibration reference data. To improve the spectrophotometric calibration of our data, we also reduce observations of the A-type standard star 2MASS J18083474+6927286 [51], taken as part of JWST commissioning programme 1128 (PI: Lützendorf) [52] using the same instrument modes. We compare the resulting stellar spectrum against a spectral model for this star from the CALSPEC library [53] to construct a calibration function, which we then apply to our observations of GS-9209.

4.2 Photometric data reduction

The majority of our photometric data are taken directly from the CANDELS GOODS South catalogue [54]. We supplement this with new JWST NIRCam photometric data taken as part of the Ultra Deep Field Medium-Band Survey [55] (Programme ID: 1963; PI: Williams). Data are available in the F182M, F210M, F430M, F460M and F480M bands. We reduce these data using the PRIMER Enhanced NIRCam Image-processing Library (PENCIL, e.g., [8]), a custom version of the JWST Science Calibration Pipeline (v1.8.0), and using version 1011 of the JWST calibration reference data. We measure photometric fluxes for GS-9209 in large, 1''-diameter apertures to ensure we measure the total flux in each band (the object is isolated, with no other sources within this radius, see Fig. 4). We measure uncertainties as the standard deviation of flux values in the nearest 100 blank-sky apertures, masking out nearby objects (e.g., [56]).

4.3 Bagpipes full spectral fitting

We fit the available photometry in parallel with our new spectroscopic data using the Bagpipes code [57]. Our model has a total of 22 free parameters, describing the stellar, dust, nebular and AGN components of the spectrum. A full list of these parameters, along with their associated priors, is given in Table 1. We fit our model to the data using the MultiNest nested sampling algorithm [58–60].

We use the 2016 updated version of the BC03 [61, 62] stellar population models, using the MILES stellar spectral library [63] and updated stellar evolutionary tracks [64, 65]. We assume a double-power-law star-formation-history model (e.g., [24, 57]). We allow the logarithm of the stellar metallicity, Z_* to vary freely from $\log_{10}(Z_*/Z_\odot) = -2.45$ to 0.55. These are the limits of the range spanned by the BC03 model grid relative to our adopted Solar metallicity value ($Z_\odot = 0.0142$ [27]).

We mask out the narrow emission lines in our spectrum during our Bagpipes fitting due to likely AGN contributions, whereas Bagpipes is only capable of modelling emission lines from star-forming regions. We do however still include a nebular model in our Bagpipes fit to allow for the possibility of nebular continuum emission from star-forming regions. We assume a stellar-birth-cloud lifetime of 10 Myr, and vary the logarithm of the ionization parameter, U , from $\log_{10}(U) = -4$ to -2 . We also allow the logarithm of the gas-phase metallicity, Z_g , to vary freely from $\log_{10}(Z_g/Z_\odot) = -2.45$ to 0.55. Because our eventual fitted model only includes an extremely small amount of star formation within the last 10 Myr for GS-9209, this nebular component makes a negligible contribution to the fitted model spectrum.

We model attenuation of the above components by dust using the model of [66, 67], which is parameterised as a power-law deviation from the Calzetti dust attenuation law [68], and also includes a Drude profile to model the 2175Å bump. We allow the V -band attenuation, A_V to vary from 0 – 4 magnitudes.

Table 1 The 22 free parameters of the Bagpipes model we fit to our spectroscopic and photometric data (see Sections 2.2 and 4.3), along with their associated prior distributions. The upper limit on τ , t_{obs} , is the age of the Universe as a function of redshift. Logarithmic priors are all applied in base ten. For parameters with Gaussian priors, the mean is μ and the standard deviation is σ .

Component	Parameter	Symbol / Unit	Range	Prior	Hyper-parameters
General	Redshift	z	(4.6, 4.7) (50, 500)	Gaussian Logarithmic	$\mu = 4.66$ $\sigma = 0.01$
	Stellar velocity dispersion	$\sigma / \text{km s}^{-1}$			
SFH	Total stellar mass formed	M_* / M_\odot	(1, 10 ¹³)	Logarithmic	
	Stellar metallicity	Z_* / Z_\odot	(0.00355, 3.55)	Logarithmic	
	Double-power-law falling slope	α	(0.01, 1000)	Logarithmic	
	Double-power-law rising slope	β	(0.01, 1000)	Logarithmic	
	Double-power-law turnover time	τ / Gyr	(0.1, t_{obs})	Uniform	
Dust	V -band attenuation	A_V / mag	(0, 4)	Uniform	
	Deviation from Calzetti slope	δ	(-0.3, 0.3)	Gaussian	$\mu = 0$ $\sigma = 0.1$
	Strength of 2175Å bump	B	(0, 5)	Uniform	
	Attenuation ratio for birth clouds	ϵ	(1, 5)	Uniform	
AGN	Power law slope ($\lambda < 5000\text{\AA}$)	$\alpha_{\lambda < 5000\text{\AA}}$	(-2.5, -0.5)	Gaussian	$\mu = -1.5$ $\sigma = 0.1$
	Power law slope ($\lambda > 5000\text{\AA}$)	$\alpha_{\lambda > 5000\text{\AA}}$	(-0.5, 1.5)	Gaussian	$\mu = 0.5$ $\sigma = 0.2$
	$\text{H}\alpha$ broad-line flux	$f_{\text{H}\alpha, \text{broad}} / \text{erg s}^{-1} \text{cm}^{-2}$	(0, 2.5×10^{-17})	Uniform	
	$\text{H}\alpha$ broad-line velocity dispersion	$\sigma_{\text{H}\alpha, \text{broad}} / \text{km s}^{-1}$	(10000, 50000)	Logarithmic	
	Continuum flux at $\lambda = 5100\text{\AA}$	$f_{5100} / \text{erg s}^{-1} \text{cm}^{-2} \text{\AA}^{-1}$	(0, 10^{-19})	Uniform	
Nebular	Ionization parameter	U	(10^{-4} , 10^{-2})	Logarithmic	
	Gas-phase metallicity	Z_g / Z_\odot	(0.00355, 3.55)	Logarithmic	
Calibration	Zero order	P_0	(0.75, 1.25)	Gaussian	$\mu = 1$ $\sigma = 0.1$
	First order	P_1	(-0.25, 0.25)	Gaussian	$\mu = 0$ $\sigma = 0.1$
	Second order	P_2	(-0.25, 0.25)	Gaussian	$\mu = 0$ $\sigma = 0.1$
Noise	White noise scaling	a	(0.1, 10)	logarithmic	

We further assume that attenuation is multiplied by an additional factor for all stars with ages below 10 Myr, and resulting nebular emission. This factor is commonly assumed to be 2, however we allow this to vary from 1 to 5.

We allow redshift to vary, using a narrow Gaussian prior with a mean of 4.66 and standard deviation of 0.01. We additionally convolve the spectral model with a Gaussian kernel in velocity space, to account for velocity dispersion in our target galaxy. The width of this kernel is allowed to vary with a logarithmic prior across a range from $50 - 500$ km s $^{-1}$.

Separately from the above components, we also include a model for AGN continuum, broad H α and H β emission. Following [37], we model AGN continuum emission with a broken power law, with two spectral indices and a break at $\lambda_{\text{rest}} = 5000\text{\AA}$ in the rest frame. We vary the spectral index at $\lambda_{\text{rest}} < 5000\text{\AA}$ using a Gaussian prior with a mean value of $\alpha_\lambda = -1.5$ ($\alpha_\nu = -0.5$) and standard deviation of 0.1. We also vary the spectral index at $\lambda_{\text{rest}} > 5000\text{\AA}$ using a Gaussian prior with a mean value of $\alpha_\lambda = 0.5$ ($\alpha_\nu = -2.5$) and standard deviation of 0.2. We parameterise the normalisation of the AGN continuum component using f_{5100} , the flux at rest-frame 5100 \AA , which we allow to vary with a linear prior from 0 to 10^{-19} erg s $^{-1}$ cm $^{-2}$ \AA^{-1} .

We model broad H α with a Gaussian component, varying the normalisation from 0 to 2.5×10^{-17} erg s $^{-1}$ cm $^{-2}$ using a linear prior, and the velocity dispersion from $1000 - 5000$ km s $^{-1}$ in the rest frame using a logarithmic prior. We also include a broad H β component in the model, which has the same parameters as the broad H α line, but with normalisation divided by the standard 2.86 ratio from Case B recombination theory. However, as shown in Fig. 2, this H β model peaks at around the noise level in our spectrum, and the line is therefore plausible in not being obviously detected in the observed spectrum.

We include intergalactic medium (IGM) absorption using the model of [69]. To allow for imperfect spectrophotometric calibration of our spectroscopic data, we also include a second-order Chebyshev polynomial (e.g., [70, 71]), which the above components of our combined model are all divided by before being compared with our spectroscopic data. We finally fit an additional white noise term, which multiplies the spectroscopic uncertainties from the JWST pipeline by a factor, a , which we vary with a logarithmic prior from 1 – 10.

4.4 Size measurement from F210M-band imaging

We model the light distribution of GS-9209 in the JWST NIRCam F210M imaging data using PetroFit [72]. We fit these PetroFit models to our data using the MultiNest nested sampling algorithm [58–60]. We use F210M in preference to the F182M band due to the smaller AGN contribution in F210M and the fact that it sits above the Balmer break, therefore being more representative of the stellar mass present rather than any ongoing star formation.

As our spectroscopic data contains strong evidence for an AGN, we fit both Sérsic and delta-function components simultaneously, convolved by an empirically estimated PSF, derived by stacking bright stars. In preliminary fitting, we find that the relative fluxes of these two components are entirely degenerate with the Sérsic parameters. We therefore predict the AGN contribution to the flux in this band based on our full-spectral-fitting result, obtaining a value of 8 ± 1 per cent. We then impose this as a Gaussian prior on the relative contributions from the Sérsic and delta function components. The 11 free parameters of our model are the overall flux normalisation, which we fit with a logarithmic prior, the effective radius, r_e , Sérsic index, n , ellipticity and position angle of the Sérsic component, the x and y centroids of both components, the position angle of the point spread function, and the fraction of light in the delta-function component, which we fit with a Gaussian prior with a mean of 8 per cent and standard deviation of 1 per cent, based on our full spectral fitting result.

Acknowledgements

The authors would like to thank James Aird for helpful discussions. A. C. Carnall thanks the Leverhulme Trust for their support via a Leverhulme Early Career Fellowship. R. J. McLure, J. S. Dunlop, D. J. McLeod, V. Wild, R. Begley, C. T. Donnan and M. L. Hamadouche acknowledge the support of the Science and Technology Facilities Council. F. Cullen acknowledges support from a UKRI Frontier Research Guarantee Grant (grant reference EP/X021025/1). A. Cimatti acknowledges support from the grant PRIN MIUR 2017 - 20173ML3WW_001.

Statement of Author Contributions

ACC led the preparation of the observing proposal, reduction and analysis of the data, and preparation of the manuscript. RJM, JSD, VW, FC and AC provided advice and assistance with data reduction, analysis and interpretation, as well as consulting on the preparation of the observing proposal. DJM, DM, RB and CTD reduced the JWST imaging data and prepared the empirical PSF. DJM, MLH and SMJ assisted with measurement of the size and morphology of GS-9209. SW assisted with selection of GS-9209 from the CANDELS catalogues prior to the observing proposal being submitted. All authors assisted with preparation of the final published manuscript.

References

- [1] Dunlop, J., Peacock, J., Spinrad, H., Dey, A., Jimenez, R., Stern, D., Windhorst, R.: A 3.5-Gyr-old galaxy at redshift 1.55. *Nature* **381**, 581–584 (1996). <https://doi.org/10.1038/381581a0>

- [2] Cimatti, A., Daddi, E., Renzini, A., Cassata, P., Vanzella, E., Pozzetti, L., Cristiani, S., Fontana, A., Rodighiero, G., Mignoli, M., Zamorani, G.: Old galaxies in the young Universe. *Nature* **430**, 184–187 (2004) [arXiv:astro-ph/0407131](https://arxiv.org/abs/astro-ph/0407131) [astro-ph]. <https://doi.org/10.1038/nature02668>
- [3] Kriek, M., Conroy, C., van Dokkum, P.G., Shapley, A.E., Choi, J., Reddy, N.A., Siana, B., van de Voort, F., Coil, A.L., Mobasher, B.: A massive, quiescent, population II galaxy at a redshift of 2.1. *Nature* **540**(7632), 248–251 (2016) [arXiv:1612.02001](https://arxiv.org/abs/1612.02001) [astro-ph.GA]. <https://doi.org/10.1038/nature20570>
- [4] Glazebrook, K., Schreiber, C., Labb  , I., Nanayakkara, T., Kacprzak, G.G., Oesch, P.A., Papovich, C., Spitler, L.R., Straatman, C.M.S., Tran, K.-V.H., Yuan, T.: A massive, quiescent galaxy at a redshift of 3.717. *Nature* **544**(7648), 71–74 (2017) [arXiv:1702.01751](https://arxiv.org/abs/1702.01751) [astro-ph.GA]. <https://doi.org/10.1038/nature21680>
- [5] Schreiber, C., Glazebrook, K., Nanayakkara, T., Kacprzak, G.G., Labb  , I., Oesch, P., Yuan, T., Tran, K.-V., Papovich, C., Spitler, L., Straatman, C.: Near infrared spectroscopy and star-formation histories of $3 < z < 4$ quiescent galaxies. *A&A* **618**, 85 (2018) [arXiv:1807.02523](https://arxiv.org/abs/1807.02523). <https://doi.org/10.1051/0004-6361/201833070>
- [6] Girelli, G., Bolzonella, M., Cimatti, A.: Massive and old quiescent galaxies at high redshift. *A&A* **632**, 80 (2019) [arXiv:1910.07544](https://arxiv.org/abs/1910.07544) [astro-ph.GA]. <https://doi.org/10.1051/0004-6361/20183454710.48550/arXiv.1910.07544>
- [7] Labbe, I., van Dokkum, P., Nelson, E., Bezanson, R., Suess, K., Leja, J., Brammer, G., Whitaker, K., Mathews, E., Stefanon, M.: A very early onset of massive galaxy formation. *arXiv e-prints*, 2207–12446 (2022) [arXiv:2207.12446](https://arxiv.org/abs/2207.12446) [astro-ph.GA]
- [8] Donnan, C.T., McLeod, D.J., Dunlop, J.S., McLure, R.J., Carnall, A.C., Begley, R., Cullen, F., Hamadouche, M.L., Bowler, R.A.A., Magee, D., McCracken, H.J., Milvang-Jensen, B., Moneti, A., Targett, T.: The evolution of the galaxy UV luminosity function at redshifts $z \simeq 8 - 15$ from deep JWST and ground-based near-infrared imaging. *MNRAS* **518**(4), 6011–6040 (2023) [arXiv:2207.12356](https://arxiv.org/abs/2207.12356) [astro-ph.GA]. <https://doi.org/10.1093/mnras/stac347210.48550/arXiv.2207.12356>
- [9] Carnall, A.C., McLeod, D.J., McLure, R.J., Dunlop, J.S., Begley, R., Cullen, F., Donnan, C.T., Hamadouche, M.L., Jewell, S.M., Jones, E.W., Pollock, C.L., Wild, V.: A first look at JWST CEERS: massive quiescent galaxies from $3 < z < 5$. *arXiv e-prints*, 2208–00986 (2022) [arXiv:2208.00986](https://arxiv.org/abs/2208.00986) [astro-ph.GA]

- [10] Valentino, F., Tanaka, M., Davidzon, I., Toft, S., Gómez-Guijarro, C., Stockmann, M., Onodera, M., Brammer, G., Ceverino, D., Faisst, A.L., Gallazzi, A., Hayward, C.C., Ilbert, O., Kubo, M., Magdis, G.E., Selsing, J., Shimakawa, R., Sparre, M., Steinhardt, C., Yabe, K., Zabl, J.: Quiescent Galaxies 1.5 Billion Years after the Big Bang and Their Progenitors. *ApJ* **889**(2), 93 (2020) [arXiv:1909.10540](https://arxiv.org/abs/1909.10540) [astro-ph.GA]. <https://doi.org/10.3847/1538-4357/ab64dc>
- [11] Caputi, K.I., Dunlop, J.S., McLure, R.J., Roche, N.D.: A deeper view of extremely red galaxies: the redshift distribution in the GOODS/CDFS ISAAC field. *MNRAS* **353**(1), 30–42 (2004) [arXiv:astro-ph/0401047](https://arxiv.org/abs/astro-ph/0401047) [astro-ph]. <https://doi.org/10.1111/j.1365-2966.2004.08044.x>
- [12] Le Fèvre, O., Tasca, L.A.M., Cassata, P., Garilli, B., Le Brun, V., Maccagni, D., Pentericci, L., Thomas, R., Vanzella, E., Zamorani, G., Zucca, E., Amorin, R., Bardelli, S., Capak, P., Cassarà, L., Castellano, M., Cimatti, A., Cuby, J.G., Cucciati, O., de la Torre, S., Durkalec, A., Fontana, A., Giavalisco, M., Grazian, A., Hathi, N.P., Ilbert, O., Lemaux, B.C., Moreau, C., Paltani, S., Ribeiro, B., Salvato, M., Schaefer, D., Scudeggio, M., Sommariva, V., Talia, M., Taniguchi, Y., Tresse, L., Vergani, D., Wang, P.W., Charlot, S., Contini, T., Fotopoulou, S., López-Sanjuan, C., Mellier, Y., Scoville, N.: The VIMOS Ultra-Deep Survey: ~10 000 galaxies with spectroscopic redshifts to study galaxy assembly at early epochs $2 < z \simeq 6$. *A&A* **576**, 79 (2015) [arXiv:1403.3938](https://arxiv.org/abs/1403.3938) [astro-ph.CO]. <https://doi.org/10.1051/0004-6361/201423829>
- [13] Merlin, E., Fontana, A., Castellano, M., Santini, P., Torelli, M., Boutsia, K., Wang, T., Grazian, A., Pentericci, L., Schreiber, C., Ciesla, L., McLure, R., Derriere, S., Dunlop, J.S., Elbaz, D.: Chasing passive galaxies in the early Universe: a critical analysis in CANDELS GOODS-South. *MNRAS* **473**(2), 2098–2123 (2018) [arXiv:1709.00429](https://arxiv.org/abs/1709.00429) [astro-ph.GA]. <https://doi.org/10.1093/mnras/stx2385>
- [14] Carnall, A.C., Walker, S., McLure, R.J., Dunlop, J.S., McLeod, D.J., Cullen, F., Wild, V., Amorin, R., Bolzonella, M., Castellano, M., Cimatti, A., Cucciati, O., Fontana, A., Gargiulo, A., Garilli, B., Jarvis, M.J., Pentericci, L., Pozzetti, L., Zamorani, G., Calabro, A., Hathi, N.P., Koekemoer, A.M.: Timing the earliest quenching events with a robust sample of massive quiescent galaxies at $2 < z < 5$. *MNRAS* **496**(1), 695–707 (2020) [arXiv:2001.11975](https://arxiv.org/abs/2001.11975) [astro-ph.GA]. <https://doi.org/10.1093/mnras/staa1535>
- [15] Santini, P., Merlin, E., Fontana, A., Magnelli, B., Paris, D., Castellano, M., Grazian, A., Pentericci, L., Pilo, S., Torelli, M.: Passive galaxies in the early Universe: ALMA confirmation of $z \sim 3 - 5$ candidates in the CANDELS GOODS-South field. *MNRAS* **486**(1), 560–569 (2019)

arXiv:1902.09548 [astro-ph.GA]. <https://doi.org/10.1093/mnras/stz801>

[16] Luo, B., Brandt, W.N., Xue, Y.Q., Lehmer, B., Alexander, D.M., Bauer, F.E., Vito, F., Yang, G., Basu-Zych, A.R., Comastri, A., Gilli, R., Gu, Q.-S., Hornschemeier, A.E., Koekemoer, A., Liu, T., Mainieri, V., Paolillo, M., Ranalli, P., Rosati, P., Schneider, D.P., Shemmer, O., Smail, I., Sun, M., Tozzi, P., Vignali, C., Wang, J.-X.: The Chandra Deep Field-South Survey: 7 Ms Source Catalogs. *The Astrophysical Journal Supplement Series* **228**, 2 (2017) arXiv:1611.03501 [astro-ph.GA]. <https://doi.org/10.3847/1538-4365/228/1/2>

[17] Bonzini, M., Padovani, P., Mainieri, V., Kellermann, K.I., Miller, N., Rosati, P., Tozzi, P., Vattakunnel, S.: The sub-mJy radio sky in the Extended Chandra Deep Field-South: source population. *MNRAS* **436**, 3759–3771 (2013) arXiv:1310.1248. <https://doi.org/10.1093/mnras/stt1879>

[18] Dunlop, J., Akiyama, M., Alexander, D., Almaini, O., Borys, C., Bouwens, R., Bremer, M., Cimatti, A., Cirasuolo, M., Clewley, L., Conselice, C., Coppin, K., Dalton, G., Damen, M., Dunne, L., Dye, S., Eales, S., Edge, A., Egami, E., Fall, M., Farrah, D., Ferguson, H., Finoguenov, A., Foucaud, S., Franx, M., Furusawa, H., Huang, J., Ibar, E., Illingworth, G., Ivison, R., Jarvis, M., Labbe, I., Lawrence, A., Maddox, S., McLure, R., Mortier, A., Oliver, S., Ouchi, M., Page, M., Papovich, C., Quadri, R., Rawlings, S., Rieke, G., Schiminovich, D., Sekiguchi, K., Serjeant, S., Simpson, C., Smail, I., Stanway, E., Taylor, A., Watson, M., Williams, R., Yamada, T., van Breukelen, C., van Dokkum, P.: A Spitzer Public Legacy survey of the UKIDSS Ultra Deep Survey. *Spitzer Proposal* (2007)

[19] Goto, T.: A catalogue of local E+A (post-starburst) galaxies selected from the Sloan Digital Sky Survey Data Release 5. *MNRAS* **381**(1), 187–193 (2007) arXiv:0801.1106 [astro-ph]. <https://doi.org/10.1111/j.1365-2966.2007.12227.x>

[20] Wild, V., Walcher, C.J., Johansson, P.H., Tresse, L., Charlot, S., Pollo, A., Le Fèvre, O., de Ravel, L.: Post-starburst galaxies: more than just an interesting curiosity. *MNRAS* **395**, 144–159 (2009) arXiv:0810.5122 [astro-ph]. <https://doi.org/10.1111/j.1365-2966.2009.14537.x>

[21] Wild, V., Taj Aldeen, L., Carnall, A., Maltby, D., Almaini, O., Werle, A., Wilkinson, A., Rowlands, K., Bolzonella, M., Castellano, M., Gar-guilo, A., McLure, R., Pentericci, L., Pozzetti, L.: The star formation histories of $z \sim 1$ post-starburst galaxies. *arXiv e-prints*, 2001–09154 (2020) arXiv:2001.09154 [astro-ph.GA]

[22] Kauffmann, G., Heckman, T.M., White, S.D.M., Charlot, S., Tremonti, C., Brinchmann, J., Bruzual, G., Peng, E.W., Seibert, M., Bernardi, M.,

Blanton, M., Brinkmann, J., Castander, F., Csabai, I., Fukugita, M., Ivezic, Z., Munn, J.A., Nichol, R.C., Padmanabhan, N., Thakar, A.R., Weinberg, D.H., York, D.: Stellar masses and star formation histories for 10^5 galaxies from the Sloan Digital Sky Survey. *MNRAS* **341**, 33–53 (2003) [arXiv:astro-ph/0204055](https://arxiv.org/abs/astro-ph/0204055) [astro-ph]. <https://doi.org/10.1046/j.1365-8711.2003.06291.x>

[23] Kroupa, P.: On the variation of the initial mass function. *MNRAS* **322**(2), 231–246 (2001) [arXiv:astro-ph/0009005](https://arxiv.org/abs/astro-ph/0009005) [astro-ph]. <https://doi.org/10.1046/j.1365-8711.2001.04022.x>

[24] Carnall, A.C., Leja, J., Johnson, B.D., McLure, R.J., Dunlop, J.S., Conroy, C.: How to Measure Galaxy Star Formation Histories. I. Parametric Models. *ApJ* **873**, 44 (2019) [arXiv:1811.03635](https://arxiv.org/abs/1811.03635) [astro-ph.GA]. <https://doi.org/10.3847/1538-4357/ab04a2>

[25] Pacifici, C., Kassin, S.A., Weiner, B.J., Holden, B., Gardner, J.P., Faber, S.M., Ferguson, H.C., Koo, D.C., Primack, J.R., Bell, E.F., Dekel, A., Gawiser, E., Giavalisco, M., Rafelski, M., Simons, R.C., Barro, G., Croton, D.J., Davé, R., Fontana, A., Grogin, N.A., Koekemoer, A.M., Lee, S.-K., Salmon, B., Somerville, R., Behroozi, P.: The Evolution of Star Formation Histories of Quiescent Galaxies. *ApJ* **832**, 79 (2016) [arXiv:1609.03572](https://arxiv.org/abs/1609.03572). <https://doi.org/10.3847/0004-637X/832/1/79>

[26] Michałowski, M.J., Dunlop, J.S., Koprowski, M.P., Cirasuolo, M., Geach, J.E., Bowler, R.A.A., Mortlock, A., Caputi, K.I., Arétxaga, I., Arumugam, V., Chen, C.-C., McLure, R.J., Birkinshaw, M., Bourne, N., Farrah, D., Ibar, E., van der Werf, P., Zemcov, M.: The SCUBA-2 Cosmology Legacy Survey: the nature of bright submm galaxies from 2 deg² of 850- μ m imaging. *MNRAS* **469**(1), 492–515 (2017) [arXiv:1610.02409](https://arxiv.org/abs/1610.02409) [astro-ph.GA]. <https://doi.org/10.1093/mnras/stx86110.48550> [arXiv.1610.02409](https://arxiv.org/abs/1610.02409)

[27] Asplund, M., Grevesse, N., Sauval, A.J., Scott, P.: The Chemical Composition of the Sun. *ARA&A* **47**(1), 481–522 (2009) [arXiv:0909.0948](https://arxiv.org/abs/0909.0948) [astro-ph.SR]. <https://doi.org/10.1146/annurev.astro.46.060407.145222>

[28] Leitherer, C., Ortiz Otálvaro, P.A., Bresolin, F., Kudritzki, R.-P., Lo Faro, B., Pauldrach, A.W.A., Pettini, M., Rix, S.A.: A Library of Theoretical Ultraviolet Spectra of Massive, Hot Stars for Evolutionary Synthesis. *ApJS* **189**(2), 309–335 (2010) [arXiv:1006.5624](https://arxiv.org/abs/1006.5624) [astro-ph.SR]. <https://doi.org/10.1088/0067-0049/189/2/309>

[29] Conroy, C., Graves, G.J., van Dokkum, P.G.: Early-type Galaxy Archaeology: Ages, Abundance Ratios, and Effective Temperatures from Full-spectrum Fitting. *ApJ* **780**(1), 33 (2014) [arXiv:1303.6629](https://arxiv.org/abs/1303.6629) [astro-ph.CO]. <https://doi.org/10.1088/0004-637X/780/1/33>

- [30] Cullen, F., McLure, R.J., Dunlop, J.S., Khochfar, S., Davé, R., Amorín, R., Bolzonella, M., Carnall, A.C., Castellano, M., Cimatti, A.: The VANDELS survey: the stellar metallicities of star-forming galaxies at 2.5 < z < 5.0. *MNRAS*, 1344 (2019) [arXiv:1903.11081](https://arxiv.org/abs/1903.11081) [astro-ph.GA]. <https://doi.org/10.1093/mnras/stz1402>
- [31] Thomas, D., Maraston, C., Bender, R., Mendes de Oliveira, C.: The Epochs of Early-Type Galaxy Formation as a Function of Environment. *ApJ* **621**, 673–694 (2005) [astro-ph/0410209](https://arxiv.org/abs/astro-ph/0410209). <https://doi.org/10.1086/426932>
- [32] Carnall, A.C., McLure, R.J., Dunlop, J.S., Hamadouche, M., Cullen, F., McLeod, D.J., Begley, R., Amorin, R., Bolzonella, M., Castellano, M., Cimatti, A., Fontanot, F., Gargiulo, A., Garilli, B., Mannucci, F., Pentericci, L., Talia, M., Zamorani, G., Calabro, A., Cresci, G., Hathi, N.P.: The Stellar Metallicities of Massive Quiescent Galaxies at $1.0 < z < 1.3$ from KMOS + VANDELS. *ApJ* **929**(2), 131 (2022) [arXiv:2108.13430](https://arxiv.org/abs/2108.13430) [astro-ph.GA]. <https://doi.org/10.3847/1538-4357/ac5b62>
- [33] Kobayashi, C., Karakas, A.I., Lugaro, M.: The Origin of Elements from Carbon to Uranium. *ApJ* **900**(2), 179 (2020) [arXiv:2008.04660](https://arxiv.org/abs/2008.04660) [astro-ph.GA]. <https://doi.org/10.3847/1538-4357/abae65>
- [34] Cullen, F., Shapley, A.E., McLure, R.J., Dunlop, J.S., Sanders, R.L., Topping, M.W., Reddy, N.A., Amorín, R., Begley, R., Bolzonella, M., Calabro, A., Carnall, A.C., Castellano, M., Cimatti, A., Cirasuolo, M., Cresci, G., Fontana, A., Fontanot, F., Garilli, B., Guaita, L., Hamadouche, M., Hathi, N.P., Mannucci, F., McLeod, D.J., Pentericci, L., Saxena, A., Talia, M., Zamorani, G.: The NIRVANDELS Survey: a robust detection of α -enhancement in star-forming galaxies at $z \simeq 3.4$. *MNRAS* **505**(1), 903–920 (2021) [arXiv:2103.06300](https://arxiv.org/abs/2103.06300) [astro-ph.GA]. <https://doi.org/10.1093/mnras/stab1340>
- [35] Chehade, B., Carnall, A.C., Shanks, T., Diener, C., Fumagalli, M., Findlay, J.R., Metcalfe, N., Hennawi, J., Leibler, C., Murphy, D.N.A., Prochaska, J.X., Irwin, M.J., Gonzalez-Solares, E.: Two more, bright, $z \gtrsim 6$ quasars from VST ATLAS and WISE. *MNRAS* **478**(2), 1649–1659 (2018) [arXiv:1803.01424](https://arxiv.org/abs/1803.01424) [astro-ph.GA]. <https://doi.org/10.1093/mnras/sty690>
- [36] Onoue, M., Kashikawa, N., Matsuoka, Y., Kato, N., Izumi, T., Nagao, T., Strauss, M.A., Harikane, Y., Imanishi, M., Ito, K., Iwasawa, K., Kawaguchi, T., Lee, C.-H., Noboriguchi, A., Suh, H., Tanaka, M., Toba, Y.: Subaru High-z Exploration of Low-luminosity Quasars (SHELLQs). VI. Black Hole Mass Measurements of Six Quasars at $6.1 \leq z \leq 6.7$. *ApJ* **880**(2), 77 (2019) [arXiv:1904.07278](https://arxiv.org/abs/1904.07278) [astro-ph.GA]. <https://doi.org/10.3847/1538-4357/ab29e9>

- [37] Vanden Berk, D.E., Richards, G.T., Bauer, A., Strauss, M.A., Schneider, D.P., Heckman, T.M., York, D.G., Hall, P.B., Fan, X., Knapp, G.R., Anderson, S.F., Annis, J., Bahcall, N.A., Bernardi, M., Briggs, J.W., Brinkmann, J., Brunner, R., Burles, S., Carey, L., Castander, F.J., Connolly, A.J., Crocker, J.H., Csabai, I., Doi, M., Finkbeiner, D., Friedman, S., Frieman, J.A., Fukugita, M., Gunn, J.E., Hennessy, G.S., Ivezić, Ž., Kent, S., Kunszt, P.Z., Lamb, D.Q., Leger, R.F., Long, D.C., Loveday, J., Lupton, R.H., Meiksin, A., Merelli, A., Munn, J.A., Newberg, H.J., Newcomb, M., Nichol, R.C., Owen, R., Pier, J.R., Pope, A., Rockosi, C.M., Schlegel, D.J., Siegmund, W.A., Smee, S., Snir, Y., Stoughton, C., Stubbs, C., SubbaRao, M., Szalay, A.S., Szokoly, G.P., Tremonti, C., Uomoto, A., Waddell, P., Yanny, B., Zheng, W.: Composite Quasar Spectra from the Sloan Digital Sky Survey. *AJ* **122**(2), 549–564 (2001) [arXiv:astro-ph/0105231](https://arxiv.org/abs/astro-ph/0105231) [astro-ph]. <https://doi.org/10.1086/321167>
- [38] Greene, J.E., Ho, L.C.: Estimating Black Hole Masses in Active Galaxies Using the H α Emission Line. *ApJ* **630**(1), 122–129 (2005) [arXiv:astro-ph/0508335](https://arxiv.org/abs/astro-ph/0508335) [astro-ph]. <https://doi.org/10.1086/431897>
- [39] Kewley, L.J., Dopita, M.A., Leitherer, C., Davé, R., Yuan, T., Allen, M., Groves, B., Sutherland, R.: Theoretical Evolution of Optical Strong Lines across Cosmic Time. *ApJ* **774**(2), 100 (2013) [arXiv:1307.0508](https://arxiv.org/abs/1307.0508) [astro-ph.CO]. <https://doi.org/10.1088/0004-637X/774/2/100>
- [40] Maltby, D.T., McLure, O.A.R.J., Wild, V., Dunlop, J., Rowlands, K., Hartley, W.G., Hatch, N.A., Socolovsky, M., Wilkinson, A., Amorin, R., Bradshaw, E.J., Carnall, A.C., Castellano, M., Cimatti, A., Cresci, G., Cullen, F., De Barros, S., Fontanot, F., Garilli, B., Koekemoer, A.M., McLeod, D.J., Pentericci, L., Talia, M.: High-velocity outflows in massive post-starburst galaxies at $z > 1$. *MNRAS*, 2140 (2019) [arXiv:1908.02766](https://arxiv.org/abs/1908.02766) [astro-ph.GA]. <https://doi.org/10.1093/mnras/stz2211>
- [41] Kennicutt, R.C., Evans, N.J.: Star Formation in the Milky Way and Nearby Galaxies. *ARA&A* **50**, 531–608 (2012) [arXiv:1204.3552](https://arxiv.org/abs/1204.3552). <https://doi.org/10.1146/annurev-astro-081811-125610>
- [42] Kormendy, J., Ho, L.C.: Coevolution (Or Not) of Supermassive Black Holes and Host Galaxies. *ARA&A* **51**(1), 511–653 (2013) [arXiv:1304.7762](https://arxiv.org/abs/1304.7762) [astro-ph.CO]. <https://doi.org/10.1146/annurev-astro-082708-101811>
- [43] McLure, R.J., Jarvis, M.J., Targett, T.A., Dunlop, J.S., Best, P.N.: On the evolution of the black hole: spheroid mass ratio. *MNRAS* **368**(3), 1395–1403 (2006) [arXiv:astro-ph/0510121](https://arxiv.org/abs/astro-ph/0510121) [astro-ph]. <https://doi.org/10.1111/j.1365-2966.2006.10228.x> [arXiv:astro-ph/0510121](https://arxiv.org/abs/astro-ph/0510121)
- [44] van der Wel, A., Franx, M., van Dokkum, P.G., Skelton, R.E., Momcheva, I.G., Whitaker, K.E., Brammer, G.B., Bell, E.F., Rix, H.-W., Wuyts,

S., Ferguson, H.C., Holden, B.P., Barro, G., Koekemoer, A.M., Chang, Y.-Y., McGrath, E.J., Häussler, B., Dekel, A., Behroozi, P., Fumagalli, M., Leja, J., Lundgren, B.F., Maseda, M.V., Nelson, E.J., Wake, D.A., Patel, S.G., Labb  , I., Faber, S.M., Grogan, N.A., Kocevski, D.D.: 3D-HST+CANDELS: The Evolution of the Galaxy Size-Mass Distribution since $z = 3$. *ApJ* **788**, 28 (2014) [arXiv:1404.2844](https://arxiv.org/abs/1404.2844). <https://doi.org/10.1088/0004-637X/788/1/28>

[45] Hamadouche, M.L., Carnall, A.C., McLure, R.J., Dunlop, J.S., McLeod, D.J., Cullen, F., Begley, R., Bolzonella, M., Buitrago, F., Castellano, M., Cucciati, O., Fontana, A., Gargiulo, A., Moresco, M., Pozzetti, L., Zamorani, G.: A combined VANDELS and LEGA-C study: the evolution of quiescent galaxy size, stellar mass, and age from $z = 0.6$ to $z = 1.3$. *MNRAS* **512**(1), 1262–1274 (2022) [arXiv:2201.10576](https://arxiv.org/abs/2201.10576) [astro-ph.GA]. <https://doi.org/10.1093/mnras/stac535>

[46] Almaini, O., Wild, V., Maltby, D.T., Hartley, W.G., Simpson, C., Hatch, N.A., McLure, R.J., Dunlop, J.S., Rowlands, K.: Massive post-starburst galaxies at $z > 1$ are compact proto-spheroids. *MNRAS* **472**, 1401–1412 (2017) [arXiv:1708.00005](https://arxiv.org/abs/1708.00005). <https://doi.org/10.1093/mnras/stx1957>

[47] Hopkins, P.F., Murray, N., Quataert, E., Thompson, T.A.: A maximum stellar surface density in dense stellar systems. *MNRAS* **401**(1), 19–23 (2010) [arXiv:0908.4088](https://arxiv.org/abs/0908.4088) [astro-ph.CO]. <https://doi.org/10.1111/j.1745-3933.2009.00777.x>

[48] Newman, A.B., Belli, S., Ellis, R.S., Patel, S.G.: Resolving Quiescent Galaxies at $z \gtrsim 2$. II. Direct Measures of Rotational Support. *ApJ* **862**(2), 126 (2018) [arXiv:1806.06815](https://arxiv.org/abs/1806.06815) [astro-ph.GA]. <https://doi.org/10.3847/1538-4357/aacd4f>

[49] Decarli, R., Walter, F., Venemans, B.P., Ba  ados, E., Bertoldi, F., Carilli, C., Fan, X., Farina, E.P., Mazzucchelli, C., Riechers, D., Rix, H.-W., Strauss, M.A., Wang, R., Yang, Y.: Rapidly star-forming galaxies adjacent to quasars at redshifts exceeding 6. *Nature* **545**(7655), 457–461 (2017) [arXiv:1705.08662](https://arxiv.org/abs/1705.08662) [astro-ph.GA]. <https://doi.org/10.1038/nature22358>

[50] Riechers, D.A., Nayyeri, H., Burgarella, D., Emonts, B.H.C., Clements, D.L., Cooray, A., Ivison, R.J., Oliver, S., P  rez-Fournon, I., Rigopoulou, D., Scott, D.: Rise of the Titans: Gas Excitation and Feedback in a Binary Hyperluminous Dusty Starburst Galaxy at $z \sim 6$. *ApJ* **907**(2), 62 (2021) [arXiv:2010.15183](https://arxiv.org/abs/2010.15183) [astro-ph.GA]. <https://doi.org/10.3847/1538-4357/abcf2e>

[51] Gordon, K.D., Bohlin, R., Sloan, G.C., Rieke, G., Volk, K., Boyer, M., Muzerolle, J., Schlawin, E., Deustua, S.E., Hines, D.C., Kraemer, K.E., Mullally, S.E., Su, K.Y.L.: The James Webb Space Telescope

Absolute Flux Calibration. I. Program Design and Calibrator Stars. AJ **163**(6), 267 (2022) [arXiv:2204.06500](https://arxiv.org/abs/2204.06500) [astro-ph.IM]. <https://doi.org/10.3847/1538-3881/ac66dc>

[52] Lützgendorf, N., Giardino, G., Alves de Oliveira, C., Zeidler, P., Ferruit, P., Jakobsen, P., Kumari, N., Rawle, T., Birkmann, S.M., Böker, T., Proffitt, C., Sirianni, M., Te Plate, M., Sohn, S.T.: Astrometric and wavelength calibration of the NIRSpec instrument during commissioning using a model-based approach. In: Coyle, L.E., Matsuura, S., Perrin, M.D. (eds.) Space Telescopes and Instrumentation 2022: Optical, Infrared, and Millimeter Wave. Society of Photo-Optical Instrumentation Engineers (SPIE) Conference Series, vol. 12180, p. 121800 (2022). <https://doi.org/10.1117/12.2630069>

[53] Bohlin, R.C., Gordon, K.D., Tremblay, P.-E.: Techniques and Review of Absolute Flux Calibration from the Ultraviolet to the Mid-Infrared. PASP **126**(942), 711 (2014) [arXiv:1406.1707](https://arxiv.org/abs/1406.1707) [astro-ph.IM]. <https://doi.org/10.1086/677655>

[54] Guo, Y., Ferguson, H.C., Giavalisco, M., Barro, G., Willner, S.P., Ashby, M.L.N., Dahlen, T., Donley, J.L., Faber, S.M., Fontana, A., Galametz, A., Grazian, A., Huang, K.-H., Kocevski, D.D., Koekemoer, A.M., Koo, D.C., McGrath, E.J., Peth, M., Salvato, M., Wuyts, S., Castellano, M., Cooray, A.R., Dickinson, M.E., Dunlop, J.S., Fazio, G.G., Gardner, J.P., Gawiser, E., Grogin, N.A., Hathi, N.P., Hsu, L.-T., Lee, K.-S., Lucas, R.A., Mobasher, B., Nandra, K., Newman, J.A., van der Wel, A.: CANDELS Multi-wavelength Catalogs: Source Detection and Photometry in the GOODS-South Field. ApJS **207**(2), 24 (2013) [arXiv:1308.4405](https://arxiv.org/abs/1308.4405) [astro-ph.CO]. <https://doi.org/10.1088/0067-0049/207/2/24>

[55] Williams, C.C., Tacchella, S., Maseda, M.V., Robertson, B.E., Johnson, B.D., Willott, C.J., Eisenstein, D.J., Willmer, C.N.A., Ji, Z., Hainline, K.N., Helton, J.M., Alberts, S., Baum, S., Bhatawdekar, R., Boyett, K., Bunker, A.J., Carniani, S., Charlot, S., Chevallard, J., Curtis-Lake, E., de Graaf, A., Egami, E., Franx, M., Kumari, N., Maiolino, R., Nelson, E.J., Rieke, M.J., Sandles, L., Shavaei, I., Simmonds, C., Smit, R., Suess, K.A., Sun, F., Ubler, H., Witstok, J.: JEMS: A deep medium-band imaging survey in the Hubble Ultra-Deep Field with JWST NIRCam & NIRISS. arXiv e-prints, 2301-09780 (2023) [arXiv:2301.09780](https://arxiv.org/abs/2301.09780) [astro-ph.GA]

[56] McLeod, D.J., McLure, R.J., Dunlop, J.S.: The $z = 9$ -10 galaxy population in the Hubble Frontier Fields and CLASH surveys: the $z = 9$ luminosity function and further evidence for a smooth decline in ultraviolet luminosity density at $z \geq 8$. MNRAS **459**(4), 3812–3824 (2016) [arXiv:1602.05199](https://arxiv.org/abs/1602.05199) [astro-ph.GA]. <https://doi.org/10.1093/mnras/stw904>

- [57] Carnall, A.C., McLure, R.J., Dunlop, J.S., Davé, R.: Inferring the star formation histories of massive quiescent galaxies with BAGPIPES: evidence for multiple quenching mechanisms. *MNRAS* **480**, 4379–4401 (2018) [arXiv:1712.04452](https://arxiv.org/abs/1712.04452). <https://doi.org/10.1093/mnras/sty2169>
- [58] Skilling, J.: Nested sampling for general bayesian computation. *Bayesian Anal.* **1**(4), 833–859 (2006). <https://doi.org/10.1214/06-BA127>
- [59] Buchner, J., Georgakakis, A., Nandra, K., Hsu, L., Rangel, C., Brightman, M., Merloni, A., Salvato, M., Donley, J., Kocevski, D.: X-ray spectral modelling of the AGN obscuring region in the CDFS: Bayesian model selection and catalogue. *A&A* **564**, 125 (2014) [arXiv:1402.0004](https://arxiv.org/abs/1402.0004) [astro-ph.HE]. <https://doi.org/10.1051/0004-6361/201322971>
- [60] Feroz, F., Hobson, M.P., Cameron, E., Pettitt, A.N.: Importance Nested Sampling and the MultiNest Algorithm. *The Open Journal of Astrophysics* **2**(1), 10 (2019) [arXiv:1306.2144](https://arxiv.org/abs/1306.2144) [astro-ph.IM]. <https://doi.org/10.21105/astro.1306.2144>
- [61] Bruzual, G., Charlot, S.: Stellar population synthesis at the resolution of 2003. *MNRAS* **344**, 1000–1028 (2003) [astro-ph/0309134](https://arxiv.org/abs/astro-ph/0309134). <https://doi.org/10.1046/j.1365-8711.2003.06897.x>
- [62] Chevallard, J., Charlot, S.: Modelling and interpreting spectral energy distributions of galaxies with BEAGLE. *MNRAS* **462**, 1415–1443 (2016) [arXiv:1603.03037](https://arxiv.org/abs/1603.03037). <https://doi.org/10.1093/mnras/stw1756>
- [63] Sánchez-Blázquez, P., Peletier, R.F., Jiménez-Vicente, J., Cardiel, N., Cenarro, A.J., Falcón-Barroso, J., Gorgas, J., Selam, S., Vazdekis, A.: Medium-resolution Isaac Newton Telescope library of empirical spectra. *MNRAS* **371**(2), 703–718 (2006) [arXiv:astro-ph/0607009](https://arxiv.org/abs/astro-ph/0607009) [astro-ph]. <https://doi.org/10.1111/j.1365-2966.2006.10699.x>
- [64] Bressan, A., Marigo, P., Girardi, L., Salasnich, B., Dal Cero, C., Rubele, S., Nanni, A.: PARSEC: stellar tracks and isochrones with the PAdova and TRieste Stellar Evolution Code. *MNRAS* **427**(1), 127–145 (2012) [arXiv:1208.4498](https://arxiv.org/abs/1208.4498) [astro-ph.SR]. <https://doi.org/10.1111/j.1365-2966.2012.21948.x>
- [65] Marigo, P., Bressan, A., Nanni, A., Girardi, L., Pumo, M.L.: Evolution of thermally pulsing asymptotic giant branch stars - I. The COLIBRI code. *MNRAS* **434**(1), 488–526 (2013) [arXiv:1305.4485](https://arxiv.org/abs/1305.4485) [astro-ph.SR]. <https://doi.org/10.1093/mnras/stt1034>
- [66] Noll, S., Pierini, D., Cimatti, A., Daddi, E., Kurk, J.D., Bolzonella, M., Cassata, P., Halliday, C., Mignoli, M., Pozzetti, L., Renzini, A., Berta, S., Dickinson, M., Franceschini, A., Rodighiero, G., Rosati, P., Zamorani, G.:

GMASS ultradeep spectroscopy of galaxies at $z \sim 2$. IV. The variety of dust populations. *A&A* **499**(1), 69–85 (2009) [arXiv:0903.3972](https://arxiv.org/abs/0903.3972) [astro-ph.CO]. <https://doi.org/10.1051/0004-6361/200811526>

[67] Salim, S., Boquien, M., Lee, J.C.: Dust Attenuation Curves in the Local Universe: Demographics and New Laws for Star-forming Galaxies and High-redshift Analogs. *ApJ* **859**(1), 11 (2018) [arXiv:1804.05850](https://arxiv.org/abs/1804.05850) [astro-ph.GA]. <https://doi.org/10.3847/1538-4357/aabf3c>

[68] Calzetti, D., Armus, L., Bohlin, R.C., Kinney, A.L., Koornneef, J., Storchi-Bergmann, T.: The Dust Content and Opacity of Actively Star-forming Galaxies. *ApJ* **533**, 682–695 (2000) [astro-ph/9911459](https://arxiv.org/abs/astro-ph/9911459). <https://doi.org/10.1086/308692>

[69] Inoue, A.K., Shimizu, I., Iwata, I., Tanaka, M.: An updated analytic model for attenuation by the intergalactic medium. *MNRAS* **442**(2), 1805–1820 (2014) [arXiv:1402.0677](https://arxiv.org/abs/1402.0677) [astro-ph.CO]. <https://doi.org/10.1093/mnras/stu936>

[70] Carnall, A.C., McLure, R.J., Dunlop, J.S., Cullen, F., McLeod, D.J., Wild, V., Johnson, B.D., Appleby, S., Davé, R., Amorin, R., Bolzonella, M., Castellano, M., Cimatti, A., Cucciati, O., Gargiulo, A., Garilli, B., Marchi, F., Pentericci, L., Pozzetti, L., Schreiber, C., Talia, M., Zamorani, G.: The VANDELS survey: the star-formation histories of massive quiescent galaxies at $1.0 < z < 1.3$. *MNRAS* **490**(1), 417–439 (2019) [arXiv:1903.11082](https://arxiv.org/abs/1903.11082) [astro-ph.GA]. <https://doi.org/10.1093/mnras/stz254410.48550/arXiv.1903.11082>

[71] Johnson, B.D., Leja, J., Conroy, C., Speagle, J.S.: Stellar Population Inference with Prospector. *ApJS* **254**(2), 22 (2021) [arXiv:2012.01426](https://arxiv.org/abs/2012.01426) [astro-ph.GA]. <https://doi.org/10.3847/1538-4365/abef6710.48550/arXiv.2012.01426>

[72] Geda, R., Crawford, S.M., Hunt, L., Bershady, M., Tollerud, E., Rantamampandy, S.: PetroFit: A python package for computing petrosian radii and fitting galaxy light profiles. *The Astronomical Journal* **163**(5), 202 (2022). <https://doi.org/10.3847/1538-3881/ac5908>